Glycobiology vol. 24 no. 1 pp. 26–38, 2014
doi:10.1093/glycob/cwt086
Advance Access publication on September 30, 2013

Shiga-like toxin binds with high avidity to multivalent O-linked blood group P1 determinants on mucin-type fusion proteins

Reeja Maria Cherian[1,2], Stefan Gaunitz[3], Anki Nilsson[4], Jining Liu[2], Niclas G Karlsson[5], and Jan Holgersson[2]

[2]Department of Clinical Chemistry and Transfusion Medicine, Sahlgrenska Academy, University of Gothenburg, SE-41345 Gothenburg, Sweden; [3]Department of Laboratory Medicine, Division of Clinical Immunology and Transfusion Medicine, Karolinska Institute, Karolinska University Hospital at Huddinge, Stockholm SE-14186, Sweden; [4]Recopharma AB, Arvid Wallgrens Backe 20, Gothenburg, Sweden; and [5]Department of Medical Biochemistry, Sahlgrenska Academy, University of Gothenburg, SE-40530 Gothenburg, Sweden

Received on June 2, 2013; revised on August 25, 2013; accepted on September 23, 2013

The binding of Shiga-like toxin 1 (Stx1) and Shiga-like toxin 2 (Stx2) to a mucin-like fusion protein, P-selectin glycoprotein ligand-1/mouse IgG_{2b} ($PSGL\text{-}1/mIgG_{2b}$), carrying multiple copies of the blood group P1 determinant on *O*-glycans was investigated with western blot and the biosensor Biacore. Chinese hamster ovary K-1 (CHO-K1) cells were stably transfected with linearized plasmids encoding the $PSGL\text{-}1/mIgG_{2b}$ fusion protein, the pigeon α1,4-galactosyltransferase (α4Gal-T) and the core 2 β1,6-*N*-acetylglucosaminyltransferase (C2GnT-I). Western blot analyses of purified $PSGL\text{-}1/mIgG_{2b}$ and liquid chromatography—mass spectrometry (LC-MS) of released *O*-glycans confirmed the presence of the P1 determinant. Western blot analysis indicated strong binding of Stx1, but not Stx2, to $PSGL\text{-}1/mIgG_{2b}$. In a Biacore assay, Stx1 and Stx2 were immobilized on a dextran chip and the binding of purified $PSGL\text{-}1/mIgG_{2b}$ and a P^k-albumin neoglycoprotein was analyzed. Stx1 and Stx2 bound with high avidity to both $PSGL\text{-}1/mIgG_{2b}$ and P^k-albumin, while the Stx1 binding was the strongest. In summary, we have shown that the pigeon α4Gal-T can be aberrantly expressed in CHO cells together with the core 2 enzyme to generate multiple, O-linked P1 determinants on a simultaneously expressed mucin-type fusion protein. P1-decorated $PSGL\text{-}1/mIgG_{2b}$ bound with high avidity to both Stx1 and Stx2, and as such constitutes a potential therapeutic inhibitor of these toxins.

Keywords: blood group P1 / mass spectrometry / mucin / Shiga-like toxin / SPR

Introduction

Shiga and Shiga-like toxins consist of a toxic A subunit and five carbohydrate binding B subunits that bind to Globotriaosylceramide (Gb3; Galα4Galβ4Glcβ1Cer). Infections by Shiga toxin-producing bacteria can cause diarrhea, hemorrhagic colitis or hemolytic uremic syndrome in infected individuals (Lindberg et al. 1987; Endo et al. 1988; Lingwood 1993; Fraser et al. 1994; Ling et al. 1998). The B subunits of the toxin attach to the terminal Galα4Galβ4-moiety of the Gb3 receptor, whereby the toxin is internalized by receptor-mediated endocytosis. Each of the five B subunit monomers can bind up to three Gb3 analogs, which accounts for a strong multivalent binding to the cell surface with up to 15 bound Gb3 molecules (Ling et al. 1998). The *N*-glycosidase activity of the A subunit inhibits protein synthesis by cleaving an adenine nucleotide from 28S RNA thereby preventing tRNA binding and subsequent chain elongation (Endo et al. 1988; Stein et al. 1992; Shimizu et al. 1998). The two immunologically distinct forms of Shiga-like toxin (Stx1) and Shiga-like toxin 2 (Stx2), also known as verotoxins due to their ability to bind to Vero cells, are mainly produced by enterohemorrhagic *Escherichia coli* and also by *Aeromononas caviae*, *Aeromononas hydrophila*, *Citrobacter freundii* and *Enterobacter cloacae* (Karmali et al. 1983; Tesh and O'Brien 1991; Johannes and Romer 2010). Stx1 is nearly identical to Shiga toxin differing by a single amino acid in the catalytic A subunit of the toxin and also recognizes Gb3. Stx2 shares 57% amino acid sequence identity with Stx1 and exists in several different forms. Most of these recognize Gb3, while one of the variants, porcine edema disease toxin (Stx2e), has been shown to bind to the glycosphingolipid Globotetraosylceramide (Gb4, *N*-acetylgalactosamine (GalNAc)β3Galα4Galβ4Glcβ1Cer) (DeGrandis et al. 1989). Recent experiments have demonstrated a slight difference in receptor specificity between the B subunits of Stx1 and Stx2, where the binding of the latter toxin, in addition to the carbohydrate determinant, is also dependent on the ceramide moiety (Gallegos et al. 2012).

Currently, the treatment for toxin-mediated effects is merely symptomatic. Clinical reports suggest that antibiotic treatment of infections of Shiga toxin-producing *Escherichia coli* may not be a suitable treatment, possibly due to release of toxins (Dundas et al. 2001). Several alternative treatment regimens have therefore been suggested, such as synthetic toxin binders, probiotic bacteria expressing Gb3 on their cell surface and monoclonal antibodies against the toxins (MacConnachie and Todd

[1]To whom correspondence should be addressed: Tel: +46-0-737749078; Fax: +46-0-31-82-84-58; e-mail: reeja.maria.cherian@gu.se; reejamaria@gmail.com

2004). Most of the synthetic Shiga toxin-binders like STAR FISH, Synsorb-P^k, SUPER TWIG and Globotriose-chitosan conjugate have been designed based on the trisaccharide moiety of Gb3 (Takeda et al. 1999; Kitov et al. 2000; Li et al. 2012).

Apart from these synthetic Gb3 analogs, pigeon egg white, which is a rich source of glycoproteins carrying the Galα4Galβ4N-acetylglucosamine (GlcNAc) (P1 epitope) sequence at the nonreducing termini of *N*-glycans, has been utilized to purify Shiga-like toxin I (Suzuki et al. 2001, 2003). It was demonstrated that Shiga-like toxin I could be purified on columns containing sepharose beads bearing pigeon egg white glycoproteins (Miyake et al. 2000; Tomoda et al. 2002). In addition, these glycoproteins have been shown to be potent and specific inhibitors of adherence mediated by the P fimbriae of uropathogenic *E. coli* (Johnson and Berggren 1993; Johnson and Ross 1994). Recently, the ability of pigeons to produce Galα4Gal linkages on glycoproteins was linked to the α4Gal-T(Gal) enzyme, which is capable of transferring a Gal residue to β galactosides on glycoproteins, unlike human α4Gal-T (Gb3 synthase) which acts on glycosylceramides (Suzuki and Yamamoto 2010).

In order to create a powerful inhibitor, a mucin-type fusion protein, P-selectin glycoprotein ligand-1/mouse IgG_{2b} (PSGL-1/mIgG_{2b}) has previously been constructed in our laboratory (Liu et al. 1997). PSGL-1/mIgG_{2b} carries 106 potential O-glycosylation sites and 6 potential N-glycosylation sites. The heavy glycosylation of the fusion protein results in a multivalent display of O-linked glycans (Liu et al. 1997). In a previous study, we have shown that the simultaneous expression of cDNAs encoding the mucin/Ig chimera and porcine α3-galactosyltransferase in COS-7 m6 cells resulted in an adsorber of xenoreactive human anti-pig antibodies that was more efficient than Galα3Gal-substituted agarose and macroporous glass beads (Liu et al. 2003). This demonstrates that multiple-binding sites on the fusion protein contributes to a stronger binding, i.e. higher avidity, compared with agarose and glass beads with conjugated carbohydrate determinants of lower density. In the present study, we have co-expressed pigeon cDNA encoding the α1,4-galactosyltransferase (α4Gal-T) together with cDNAs encoding PSGL-1/mIgG_{2b} and the core 2 β1,6-*N*-acetylglucosaminyltransferase (C2GnT-I) in Chinese hamster ovary K-1 (CHO-K1) cells. The resulting cell line produced a recombinant mucin-type fusion protein carrying the P1 carbohydrate determinant (Galα4Galβ4GlcNAc) on its *O*-glycans. We demonstrate the binding of Stx1 and Stx2 to PSGL-1/mIgG_{2b} carrying the P1 epitope using western blotting and surface plasmon resonance (SPR). This recombinant fusion protein may thus potentially function as an inhibitor of Shiga and Shiga-like toxins binding to host cells, thereby offering an opportunity for therapeutic intervention.

Results

Stable expression of P1-substituted PSGL-1/mIgG_{2b} in CHO cells

CHO cells stably co-transfected with the expression vectors encoding PSGL-1/mIgG_{2b}, C2GnT-I and pigeon α4Gal-T (C-PP1) were analyzed by immunocytochemistry to confirm the expression of PSGL-1/mIgG_{2b} and carbohydrate P1 epitope (Figure 1A and C). All the 4′,6-diamidino-2-phenylindole (DAPI)-stained cells were positive for staining with fluorescein isothiocyanate (FITC)-conjugated goat anti-mouse IgG (Fc) antibody (Figure 1A) and a mouse monoclonal anti-P1 antibody followed by a secondary FITC-conjugated goat anti-mouse IgM antibody (Figure 1C) indicating a high frequency of PSGL-1/mIgG_{2b} and P1 epitope expression in the selected C-PP1 clones. False-positive staining was ruled out by staining nontransfected CHO-K1 cells and CHO-K1 cells transfected with PSGL-1/mIgG_{2b} and C2GnT-I as respective negative controls (Figure 1B and D).

PSGL-1/mIgG_{2b} produced in CHO-K1 cells is expressed as a dimer and carry the carbohydrate determinant P1

Two highly expressing C-PP1 clones (C-PP1-A1 and C-PP1-A11) were chosen based on the concentration of fusion protein and its relative level of P1 substitution as assessed by enzyme-linked immunosorbent assay (ELISA) and western blot, respectively. Sodium dodecyl sulfate–polyacrylamide gel electrophoresis (SDS–PAGE) and western blot analyses on PSGL-1/mIgG_{2b} purified from C-PP1-A1 and C-PP1-A11 by protein A affinity chromatography and gel filtration revealed a protein of 250–350 kDa under nonreducing conditions (Figure 2A–C). In accordance with previous observations (Liu et al. 1997, 2003; Gustafsson et al. 2011), PSGL-1/mIgG_{2b} was produced as a dimer as indicated by the size of the protein stained by mouse IgG Fc-specific (Figure 2A, Lanes 1–4) and PSGL-1-specific (Figure 2B, Lanes 1–4) antibodies. Both anti-IgG(Fc) and anti-CD162 (which recognizes PSGL-1) stains purified PSGL-1/mIgG_{2b} produced in C-PP1 (Lanes 1–4) and C-P55 (CHO-K1 transfected with cDNA encoding PSGL-1/mIgG_{2b} only, Lane 5) clones. The top band represents the fusion protein dimer, while lower bands represent fusion protein monomers and breakdown products. Expression of C2GnT-I can be verified by an increase in size of PSGL-1/mIgG_{2b} due to more complex glycans on the fusion protein produced from C-PP1 clones (Figure 2A and B, Lanes 1 and 3) compared with the C-P55 clone (Figure 2A and B, Lane 5). The presence of P1 determinants on the fusion protein was verified using the anti-P1 antibody. This antibody, which recognizes terminal Galα1,4Galβ1,4GlcNAc, stains strongly the C-PP1-produced PSGL-1/mIgG_{2b} (Figure 2C, Lane 1 and 3) as well as P1 determinant conjugated to bovine serum albumin (P1-BSA) (Figure 2C, Lane 6), but not C-P55-produced PSGL-1/mIgG_{2b} (Figure 2C, Lane 5). Thus, co-expression of the pigeon α4Gal-T led to expression of the P1 determinant on the fusion protein. C-PP1-produced PSGL-1/mIgG_{2b} also reacted with GSA I IB_4 lectin, but not with an anti-P^k antibody (data not shown). A staining kit (Pro Q Emerald) that stains glycoproteins was used in combination with Ruby total protein stain to detect glycosylated as well as nonglycosylated proteins. The Candycane precision standard (Invitrogen, Carlsbad, CA) was applied as a reference for protein molecular weight determination. The purified PSGL-1/mIgG_{2b} fractions did not contain any significant amounts of glycosylated or nonglycosylated contaminating proteins (Figure 2D and E).

The majority of the P1 determinants are carried on O-linked glycans on PSGL-1/mIgG_{2b}

In order to confirm that the P1 determinants on PSGL-1/mIgG_{2b} were located on O-linked and not on N-linked glycans,

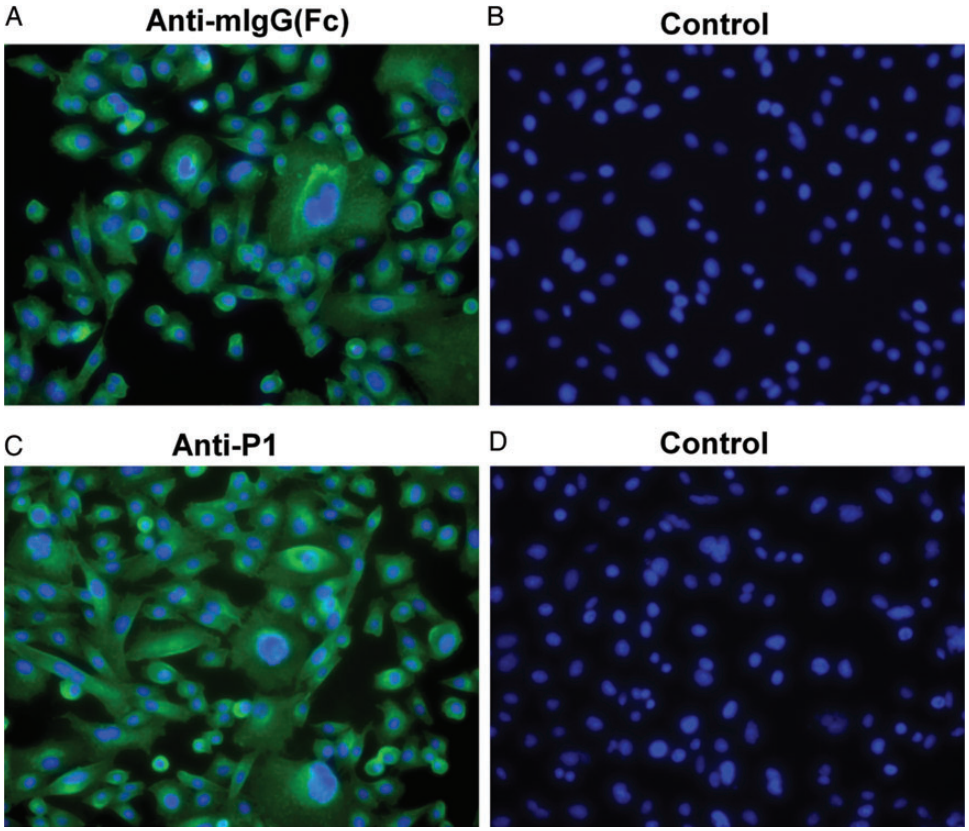

Fig. 1. Immunocytochemistry staining of CHO cells stably co-transfected with PSGL-1/mIgG$_{2b}$, C2GnT-I and pigeon α4Gal-T. C-PP1 cells (**A**) and nontransfected CHO cells (**B**) were stained with DAPI and FITC-conjugated goat anti-mouse IgG (Fc) antibody for detection of PSGL-1/mIgG$_{2b}$ expression. P1 expression was confirmed by staining C-PP1 cells with a mouse monoclonal anti-P1 antibody followed by a secondary FITC-conjugated goat anti-mouse IgM antibody and DAPI (**C**). C-P55 cells with core 2 expression were used as negative control for P1 expression (**D**).

the purified fusion protein produced in clone C-PP1-A1 and C-PP1-A11 was digested with *N*-glycosidase F (PNGase F), which completely removed N-linked glycans. SDS–PAGE and western blot analyses using anti-mouse IgG(Fc) and anti-CD162 (PSGL-1) revealed efficient cleavage of the *N*-glycans, confirmed by a mobility shift of PSGL-1/mIgG$_{2b}$ following PNGaseF treatment (Figure 2A and B, Lanes 1 and 2, Lanes 3 and 4). Anti-P1 binding resisted PNGase F treatment (Figure 2C, Lanes 2 and 4) and there was no significant reduction in anti-P1 antibody staining intensity, suggesting that the majority of this carbohydrate determinant is carried by O-linked glycans.

LC-MS of released O-glycans

O-glycans were released by reductive β-elimination from affinity- and size exclusion chromatography-purified PSGL-1/mIgG$_{2b}$ produced in C-PP1. The non-derivatized, reduced *O*-glycans were analyzed with liquid chromatography—mass spectrometry (LC-MS) in negative ion mode. The graphitized carbon column separated the *O*-glycans with an increasing acetonitrile gradient and the glycans were detected by full scans (*m*/*z* 383–2000) followed by MS^2 scans of the most intense ions. This allows the collection of MS^2 spectra of most separated glycans. The MS^2 spectra of all annotated spectra in this report have been submitted to the UniCarb-DB (http://www.unicarb-db.org/) for public access. The MS/MS data suggest that the major ions in the composite spectrum, *m*/*z* 1040.3 and *m*/*z* 1331.3/665.3^{2-}, represent tentative *N*-acetyl lactosamine on core 2 with one or both chains terminated with sialic acid (Sia) (Figure 3A). These structures confirm the successful transfection of the β1,6 *N*-acetylglucosaminyltransferase (core 2) cDNA, which together with an endogenous β1,4 galactosyltransferase support the biosynthesis of a single type 2 *N*-aceyllactosamine unit.

The major ion at *m*/*z* 1202.4 can be explained by a sugar composition suggesting the presence of a core 2 structure terminated by Sia on one of the branches and a hexose (Hex) on the other, i.e. a tentative Galα4Galβ4GlcNAcβ6(NeuAcα3Galβ3) GalNAcol *O*-glycan. This structure is expected following expression of the core 2 enzyme and the pigeon α4Gal-T. In support of this structure, the MS^2 spectrum of *m*/*z* 1202.4 (RT 23.5 min) is dominated by *m*/*z* 911.3 ([M–NeuAc]$^-$) and the Z/Y cleavage pair *m*/*z* 731.3/749.3 ([M–NeuAc–Hex]$^-$) (Figure 3B). The presence of an intense Z ion suggests the loss of the C-3 branch, indicating that the Galα4Galβ4GlcNAc moiety is located on C-6 of the GalNAcol. The MS^2 daughter ion *m*/*z* 407.2 ([M–3 Hex–NeuAc]$^-$) may only stem from a core 2 structure. While the diagnostic fragment ions $^{0,2}A_{2\alpha}$ and $^{0,2}A_{2\alpha}$—H_2O indicating an 1,4-linkage of Hex (Schulz et al. 2002) were not identified in

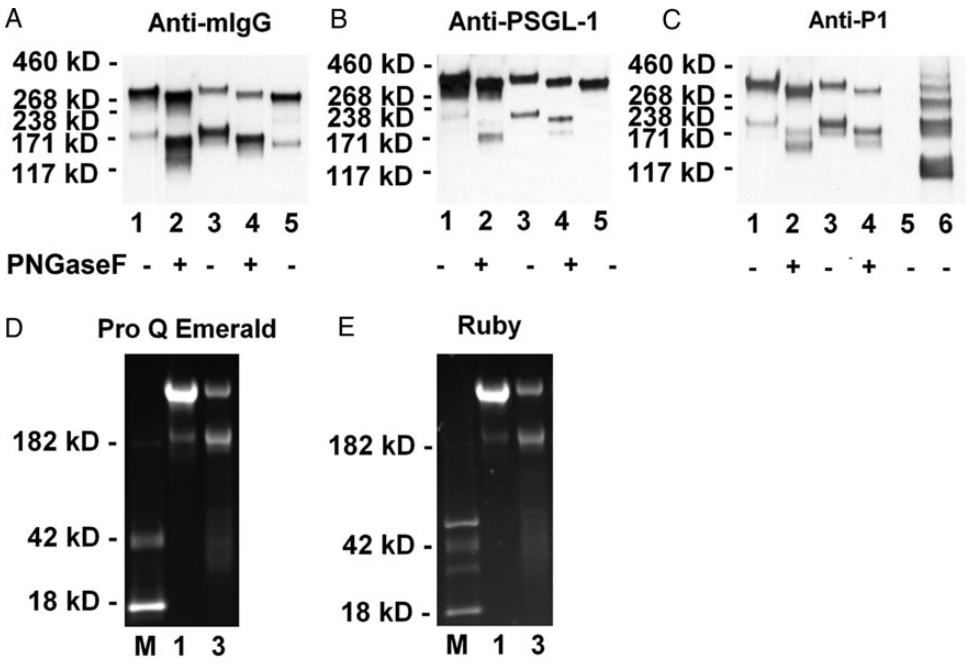

Fig. 2. SDS–PAGE and western blot analysis of purified PSGL-1/mIgG$_{2b}$ carrying blood group P1 determinants. P1-substituted PSGL-1/mIgG$_{2b}$ [clone C-PP1-A1 non-treated (Lane 1) and PNGase F-treated (Lane 2); clone C-PP1-A11 non-treated (Lane 3) and PNGase F-treated (Lane 4)], PSGL-1/mIgG$_{2b}$ carrying mono- and disialylated core 1 *O*-glycans [clone C-P55 (Lane 5)], P1-BSA (Lane 6) and Candycane precision standard (Lane M) were separated by SDS–PAGE under nonreducing conditions. For western blot analyses, 200 ng of protein was loaded per well and membranes were probed with anti-mIgG(Fc) (**A**), anti-PSGL-1 (**B**) and anti-P1 antibodies (**C**). Five micrograms of protein were loaded per well for chemical detection of proteins; glycosylated proteins were detected by Pro Q Emerald (**D**) and all proteins by Ruby (**E**).

the sialylated version, these fragment ions were found in the MS^2 spectrum of the minor ion at *m/z* 911.2 (RT 18.8 min) with *m/z* ratios of 280.9 and 263.1, respectively. In conclusion, based on the availability of glycosyltransferases in the cell line and the MS data, we suggest that the C-PP1 cell clone produce the P1 determinant, represented by the mono-sialylated glycan Galα4Galβ4GlcNAcβ6(NeuAcα3Galβ3)GalNAcol (*m/z* 1202.4) and a minor nonsialylated glycan Galα4Galβ4GlcNAcβ6(Galβ3) GalNAcol (*m/z* 911.3).

Stx1 binds with high affinity to PSGL-1/mIgG$_{2b}$ carrying the P1 determinant

SDS–PAGE and western blot analysis were performed to evaluate the ability of P1-substituted PSGL-1/mIgG$_{2b}$ to bind Stx1. Western blot membranes were probed with highly purified Stx1 (95%) at a concentration of 0.5 µg/mL (Figure 4A) and partially purified Stx1 (50%) at 1 µg/mL concentration (Figure 4B). On the first membrane (Figure 4A), only 250 ng of fusion protein was loaded, whereas in the second membrane fusion protein concentration was increased to 1 µg (Figure 4B). In summary, fusion protein produced from C-PP1 clones reacted strongly with Stx1 (Figure 4A and B, Lanes 1 and 2). However, PSGL-1/mIgG$_{2b}$ produced in the C-PP1-A1 when compared with the C-PP1-A11 clone stained considerably stronger with Stx1, and highly purified Stx1 binds more efficiently compared with the partially purified toxin. Stx1 binds to the positive control (P^k-human serum albumin (HSA) (500 ng), Lane 5), but not to PSGL-1/mIgG$_{2b}$ produced in C-P55 cells (500 ng, Lane 3), which lacks the P1 determinant. As can be seen, partially purified Stx1 does not bind to the P1-BSA ((500 ng), Figure 4B, Lane 4), while slight binding of highly purified Stx1 to P1-BSA was detected (Figure 4A, Lane 4). Furthermore, the toxin binding to the fusion protein was comparatively stronger than binding to the positive control, P^k-HSA. The ability of the fusion protein carrying the P1 determinant to bind Stx2 was also evaluated. There was no significant binding of Stx2 to the fusion protein, P^k-HSA or P1-BSA (data not shown). This result reflects that Stx2 binds with much lower affinity to P^k-HSA and C-PP1 PSGL-1/mIgG$_{2b}$, because some binding was observed in the Biacore assay (see next section).

Stx1 and Stx2 bind with high avidity to P1-carrying PSGL-1/mIgG$_{2b}$ and P^k-HSA as assessed by SPR

In order to monitor the interaction of C-PP1-produced PSGL-1/mIgG$_{2b}$ and Shiga-like toxins, a SPR assay was setup. During injection of the fusion protein (analyte) over the immobilized Stx1 or Stx2 protein (ligand), the association (complex formation) and dissociation (complex decay) was monitored in real-time using a CM5 chip with a Biacore 2000 instrument. The sensorgrams of the C-PP1 fusion protein and P^k-HSA injected over the Stx1 surface (0.14–2700 nM) are shown in Figure 5A and B. The same Stx1 surface was used for both the C-PP1-produced PSGL-1/mIgG$_{2b}$ and P^k-HSA experiments in order to facilitate direct comparison of the binding. The binding curves of the C-PP1 fusion protein and P^k-HSA were similar, but the binding response of C-PP1 PSGL-1/mIgG$_{2b}$ was slightly higher and the dissociation a little slower (cp. Figure 5A and B). Molecular weight-adjusted curves (RU/MW × 1000)

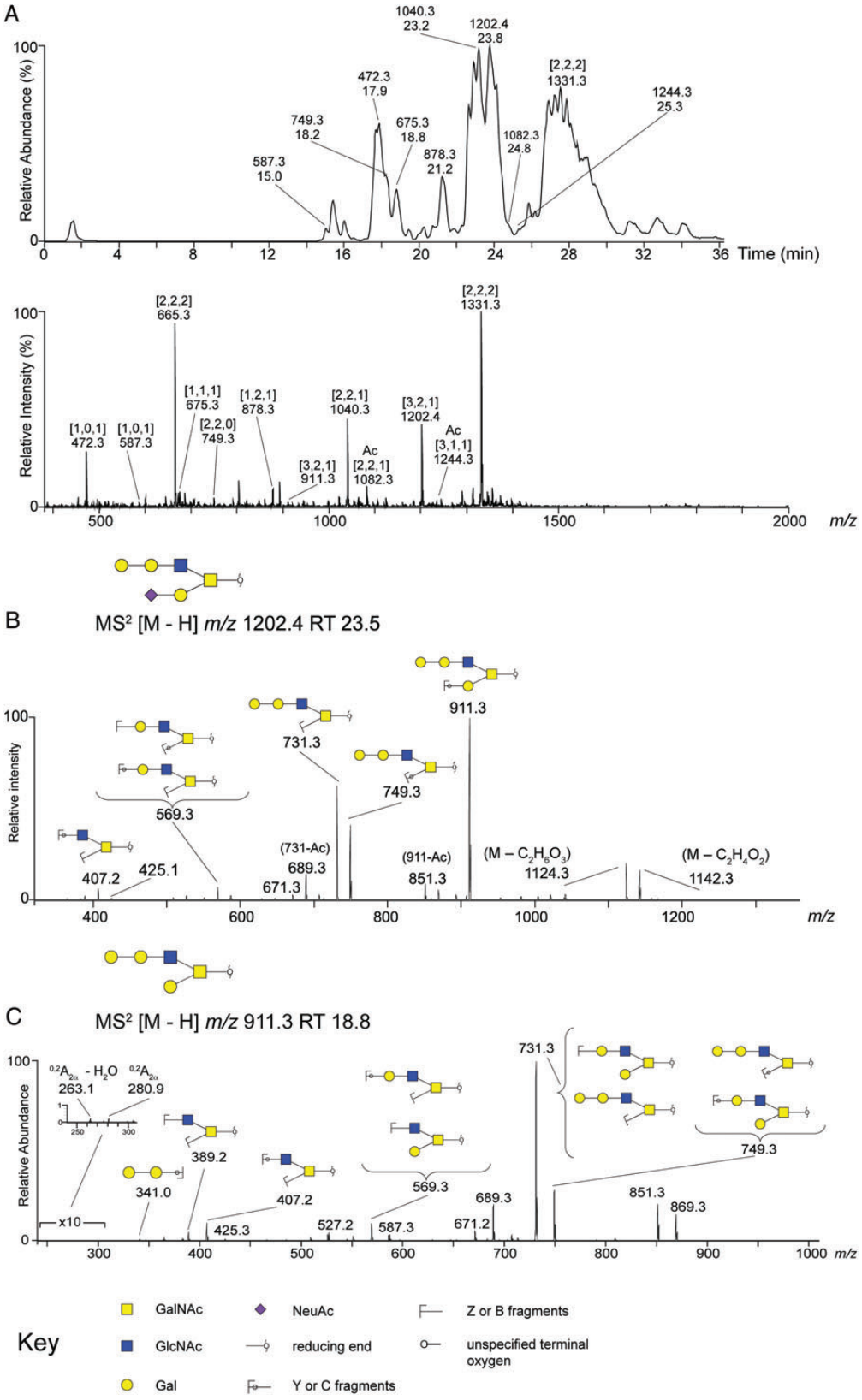

Fig. 3. LC-MS chromatogram and spectra in negative mode of *O*-glycan oligosaccharide alditols released from PSGL-1/mIgG_{2b} produced in C-PP1 cells. The mass and retention times of major *O*-glycans are annotated in the base peak chromatogram and their compositions are assigned in the spectrum using the [Hex, *N*-acetylhexosamine (HexNAc), Sia] format with reducing end GalNAcol included as HexNAc (**A**). Tentative carbohydrate structures are depicted with cartoons (Varki et al. 2009) in the LC-MS^2 spectra of the *m*/*z* 1202.4 [M–H] ion (**B**) and the *m*/*z* 911.3 [M–H] ion (**C**).

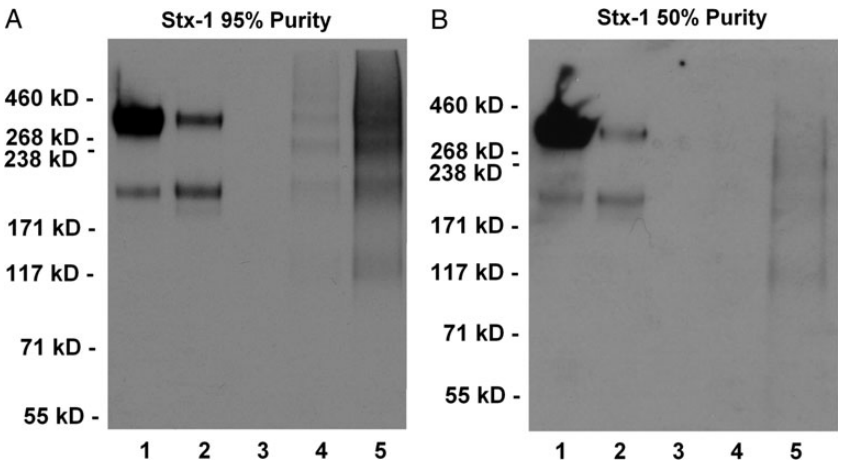

Fig. 4. Western blot analysis of CHO-K1-produced PSGL-1/mIgG$_{2b}$ carrying blood group P1 determinants using Stx1. P1-substituted PSGL-1/mIgG$_{2b}$ (Lane 1: C-PP1-A1; Lane 2: C-PP1-A11), mono- and disialylated core 1-substituted PSGL-1/mIgG$_{2b}$ (Lane 3: CP-55, negative control), P1-BSA (Lane 4, positive control) and P^k-HSA (Lane 5, positive control) were separated by SDS–PAGE under nonreducing conditions. Following western blotting, the membranes were probed with highly (**A**, 0.5 μg/mL) or partially (**B**, 1 μg/mL) purified Stx1. In panel (**A**), 250 ng of P1-substituted PSGL-1/mIgG$_{2b}$ was loaded and in panel (**B**) 1 μg. In both panels, 500 ng of positive and negative controls were loaded per well.

indicate that the relative binding of P^k-HSA was higher (cp. Figure 5C and D). The response signal is directly proportional to the mass of injected analyte and the masses of C-PP1 PSGL-1/mIgG$_{2b}$ (∼300 kDa) and P^k-HSA (73.5 kDa) are different. After 10 min of analyte injection, high concentration curves had a marked reduction in curvature as the surface started to saturate, while the lower concentration curves did not reach steady-state. The dissociation phase (injection of buffer) was markedly slow with only a slight loss of response signal after 10 min. The shape of the binding curves was not consistent with simulated 1:1 binding curves. This indicates that the binding of C-PP1 PSGL-1/mIgG$_{2b}$ and P^k-HSA to Stx1 is more complex. Therefore, the dissociation equilibrium constant, K_D, was estimated by plotting the response at the end of the injections (550–600 s) against the analyte concentration using a simple 1:1 model fit available in the Scrubber 2 software (Table I). The fitted concentration plots of C-PP1 PSGL-1/mIgG$_{2b}$ and P^k-HSA are shown in Figure 5E and F, respectively. The apparent K_D values for C-PP1 PSGL-1/mIgG$_{2b}$ and P^k-HSA were similar, $15.5 \pm 0.2 \times 10^{-9}$ M and $39.2 \pm 0.4 \times 10^{-9}$ M, respectively. Since the interactions between the analytes and ligands are multivalent, these values represent the combined strength of the binding, i.e. the avidity. The K_D values may be slightly underestimated, because all curves did not reach steady-state. The dissociation constant, k_d, was estimated by fitting only the dissociation phase of the curves (600–1200 s) to a 1:1 model in the Scrubber 2 software. The simulated 1:1 dissociation curves in orange are overlaid in the sensorgrams in Figure 5A–D. The C-PP1 PSGL-1/mIgG$_{2b}$ and P^k-HSA k_d values obtained were $1.4 \pm 0.01 \times 10^{-4}$ s^{-1} and $3.4 \pm 0.01 \times 10^{-4}$ s^{-1}, respectively. The half-life of the ligand-analyte complex was very short, $t_{1/2}$ 4836 s (C-PP1 PSGL-1/mIgG$_{2b}$) and 2040s (P^k-HSA), respectively. The association constant, k_a, was determined by dividing k_d by K_D; 9.2×10^3 M^{-1} s^{-1} (C-PP1 PSGL-1/mIgG$_{2b}$) and 8.7×10^3 M^{-1} s^{-1} (p^k-HSA), respectively.

We also immobilized Stx2 on a CM5 chip surface and monitored the binding of C-PP1 PSGL-1/mIgG$_{2b}$ and P^k-HSA. In contrast to the western blot experiment, some C-PP1 PSGL-1/mIgG$_{2b}$ and P^k-HSA binding was observed to Stx2 (Figure 6A–F). The weaker binding did not result in steady-state curves or saturation of the surfaces within 10 min of injection. This indicates that Stx2 binds with lower affinity than Stx1 to C-PP1 PSGL-1/mIgG$_{2b}$ and P^k-HSA. The curves were not suitable for steady-state calculation of the equilibrium dissociation constant K_D; rather, the association and dissociation sections of the curves were fitted to a 1:1 model. The fitted simulated curves of C-PP1 PSGL-1/mIgG$_{2b}$ (A and C) and P^k-HSA (B and D) are overlaid in Figure 6. The apparent equilibrium dissociation constant K_D values were markedly higher than the values obtained from the Stx1 surfaces: C-PP1 PSGL-1/mIgG$_{2b}$; $379 \pm 5 \times 10^{-9}$ M and P^k-HSA; $101.3 \pm 0.4 \times 10^{-9}$ M (Table I). Internal controls lacking the P^k or P1 glycan epitopes (PSGL-1/mIgG$_{2b}$ produced in wild-type CHO-K1 (C-P55) and HSA-Sia-LAcNAc) did not bind to the Stx1 or Stx2 surfaces. The binding responses of 2700 nM injections are included as red diamonds in the concentration plots Figures 5E and F and 6E and F. The lack of binding of the controls indicates that the observed C-PP1 PSGL-1/mIgG$_{2b}$ and P^k-HSA binding is explained with the presence of specific carbohydrate receptors and not the protein backbone.

Discussion

Multivalent carbohydrate-based ligands that can inhibit biomedically important protein–carbohydrate interactions have huge therapeutic potential. In this study, we have established stable CHO cell lines that generated blood group P1-substituted mucin-type fusion proteins with high Stx1-binding avidity. Our ligand is structurally versatile compared with other synthetic Shiga toxin binders and carries multiple copies of the P1 trisaccharide (Galα1,4Galβ1,4GlcNAc) on core 2 chain *O*-glycans. The binding of Stx1 and Stx2 to C-PP1 PSGL-1/mIgG$_{2b}$, P1-BSA and P^k-HSA neoglycoconjugates was probed by western blotting (Figure 4) and Biacore SPR experiments

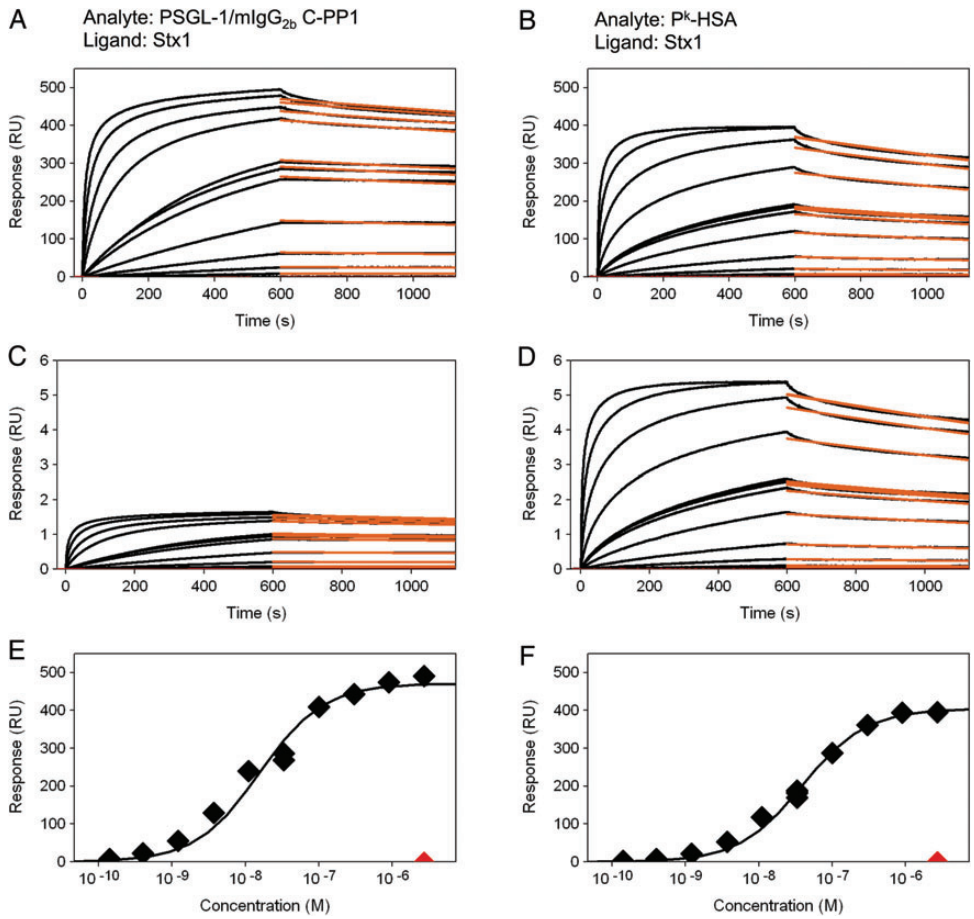

Fig. 5. SPR sensorgrams representing C-PP1 PSGL-1/mIgG$_{2b}$ and P^{k}-HSA binding to immobilized Stx1. C-PP1 PSGL-1/mIgG$_{2b}$ (**A**) and (**C**) and P^{k}-HSA (**B**) and (**D**) sensorgrams are shown where (**C**) and (**D**) are derived from (**A**) and (**B**) by adjusting the response curves for the molecular weight of the analytes (RU/molecular weight of analyte × 1000). In order to determine the equilibrium dissociation constant (K_D) of C-PP1 PSGL-1/mIgG$_{2b}$ and P^{k}-HSA, the equilibrium segments of the curves in (**A**) and (**C**) (550–600 s) were plotted against the log analyte concentrations, as seen in (**E**) and (**F**), respectively. Curves (**A**–**D**) are overlaid with the simulated dissociation curves based on a 1:1 model (orange). Negative controls, C-P55-derived PSGL-1/mIgG$_{2b}$ and Sia-LacNAc-HSA, are shown as red diamonds in (**E**) and (**F**). Concentrations of injected analytes: 0.14, 0.4, 1.2, 3.7, 11, 33, 100, 300, 900 and 2700 nM.

Table I. Kinetic constants of PSGL-1/mIgG$_{2b}$ and neoglycoconjugate P^{k}-HSA binding to Stx1 and Stx2

Analyte	Association constant (k_a) (M^{-1} s^{-1})	Dissociation constant (k_d) (s^{-1})	Equilibrium dissociation constant (K_D) (M)	Half-life $t_{1/2}$ ($\ln 2/k_d$) (s)
Stx1				
C-PP1-produced PSGL-1/mIgG$_{2b}$	9.2×10^{3}[a]	$1.4 \pm 0.01 \times 10^{-4}$[c]	$15.5 \pm 0.2 \times 10^{-9}$[e]	4836[g]
P^{k}-HSA	8.7×10^{3}[a]	$3.4 \pm 0.01 \times 10^{-4}$[c]	$39.2 \pm 0.4 \times 10^{-9}$[e]	2040[g]
Stx2				
C-PP1-produced PSGL-1/mIgG$_{2b}$	$0.4 \times 10^{3} \pm 0.01$[b]	$1.6 \pm 0.02 \times 10^{-4}$[d]	$379 \pm 5 \times 10^{-9}$[f]	4214[h]
P^{k}-HSA	$1.5 \times 10^{3} \pm 0.01$[b]	$1.5 \pm 0.01 \times 10^{-4}$[d]	$101.3 \pm 0.4 \times 10^{-9}$[f]	4732[h]

[a]k_a was calculated from K_d and K_D.
[b]k_a was calculated from fitted association curves.
[c]k_d was calculated from fitted dissociation curves.
[d]k_d was calculated from fitted dissociation curves.
[e]K_D was calculated from fitted steady-state curves.
[f]K_D was calculated from k_d and k_a.
[g]Half-life was calculated from k_d.

(Figures 5 and 6). Western blotting experiments showed that both C-PP1 PSGL-1/mIgG$_{2b}$ and P^{k}-HSA bound strongly to Stx1 while P1-BSA bound only weakly. The stronger stain of C-PP1 PSGL-1/mIgG$_{2b}$ compared with P1-BSA neoglycoconjugate may be due to its high Galα1,4Gal epitope density. The use of a mucin-type fusion protein as a scaffold

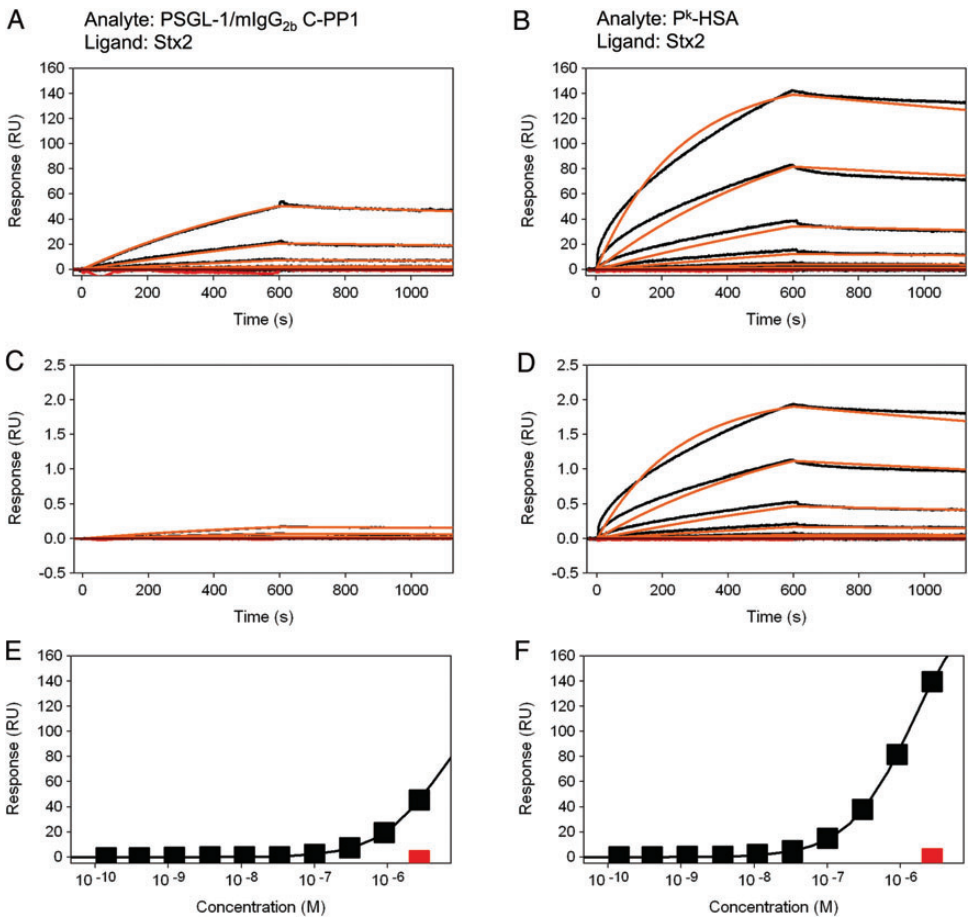

Fig. 6. SPR sensorgrams representing C-PP1 PSGL-1/mIgG$_{2b}$ and P^k-HSA binding to immobilized Stx2. C-PP1 PSGL-1/mIgG$_{2b}$ (**A** and **C**) and P^k-HSA (**B**) and (**D**) sensorgrams are shown where (**C**) and (**D**) are derived from (**A**) and (**B**) by adjusting the response curves for the molecular weight of the analytes (RU/molecular weight of analyte × 1000). In order to determine the equilibrium dissociation constant (K_D) of C-PP1 PSGL-1/mIgG$_{2b}$ and P^k-HSA, the equilibrium segments of the curves in (**A**) and (**C**) (550–600 s) were plotted against the log analyte concentrations, as seen in (**E**) and (**F**), respectively. Curves (**A**–**D**) are overlaid with the simulated dissociation curves based on a 1:1 model (orange). Negative controls, C-P55-derived PSGL-1/mIgG$_{2b}$ and Sia-LacNAc-HSA, are shown as red rectangles in panel (**E**) and (**F**). Concentrations of injected analytes: 0.14, 0.4, 1.2, 3.7, 11, 33, 100, 300, 900 and 2700 nM.

enabled multivalent presentation of the bioactive P1 determinant on core 2 *O*-glycans. Stx2 was probed in the same manner but no binding was observed to C-PP1 PSGL-1/mIgG$_{2b}$, P^k-HSA or P1-BSA (data not shown). In agreement with the western blot experiments strong binding of Stx1 to C-PP1 PSGL-1/mIgG$_{2b}$ and P^k-HSA was also observed in an SPR assay (Figure 5A and B). Dividing the binding response with the molecular weight yields a stronger relative response for P^k-HSA than C-PP1 PSGL-1/mIgG$_{2b}$ (Figure 5C and D). Even though fewer C-PP1 PSGL-1/mIgG$_{2b}$ molecules are bound to the surface, the calculated apparent dissociation equilibrium constant (K_D) is in the low nanomolar range for both C-PP1 PSGL-1/mIgG$_{2b}$ ($15.5 \pm 0.2 \times 10^{-9}$ M) and P^k-HSA ($39.2 \pm 0.4 \times 10^{-9}$ M). C-PP1 PSGL-1/mIgG$_{2b}$, P^k-HSA and Stx1 have multiple-binding sites that are not accounted for in the simple 1:1 binding model. In fact, no model exists that includes as many possible binding sites as we have in our analyte-ligand combinations. Further, the exact valency of the analytes and immobilized ligand is not known in our system. The calculated values are, therefore, estimations of avidity and most suitable for comparisons between C-PP1 PSGL-1/mIgG$_{2b}$ and P^k-HSA. The faster decay (k_d) of the P^k-HSA-Stx1 complex accounts for the main difference in K_D compared with C-PP1 PSGL-1/mIgG$_{2b}$-Stx1 (Table I). The binding of Stx2 to C-PP1 PSGL-1/mIgG$_{2b}$ (K_D $379 \pm 5 \times 10^{-9}$ M) and P^k-HSA (K_D $101.3 \pm 0.4 \times 10^{-9}$ M) was markedly weaker than the Stx1 binding. Interestingly, Stx2 clearly bound stronger to P^k-HSA than to C-PP1 PSGL-1/mIgG$_{2b}$. Comparing the kinetic constants of all the analyte-ligand pairs, it becomes apparent that the main difference in the K_D values are explained with the slow association (k_a) of Stx2 compared with Stx1, since the dissociation (k_d) values are similar (Table I). The negative controls, C-P55-derived PSGL-1/mIgG$_{2b}$ and Sia-LacNAc-HSA that do not carry the P1 or P^k glycans, did not bind to Stx1 or Stx2. This indicates that the Stx1 and Stx2 binding curves are mainly explained with the presence of specific P1 and P^k glycans on the analytes. In summary, C-PP1 PSGL-1/mIg$_{2b}$ is a good binder of Stx1 and displays a slow dissociation, which is probably explained with multivalent binding between Stx1 and C-PP1 PSGL-1/mIg$_{2b}$. Even though the Stx2 binding to C-PP1 PSGL-1/mIg$_{2b}$ was almost 25 times weaker than Stx1 binding, the calculated K_D is still comparatively low. The difference in avidity may explain the lack of binding of Stx2 in the

immunoblotting experiment, but it is also possible that the probing on the membrane was less favorable for the Stx2 toxin compared with Stx1. In vitro studies of Stx1 and Stx2 have indicated that ELISA is more sensitive than SPR (Flagler et al. 2010). In this study, the SPR assay was more sensitive than immunoblotting. Even though several reports hold P^k as the best Stx1 receptor (Lindberg et al. 1987; Flagler et al. 2010), it has been shown that Stx1 bound better to a glycan that differed from P^k by the presence of *N*-acetylation of the third sugar residue, suggesting that the P1 trisaccharide may be the preferred glycan for Stx1 binding (Gallegos et al. 2012). It should be noted that in contrast to the human P^k and P1 antigens that exist mostly on glycosphingolipids, P1 is also found on glycoproteins in certain bird species (Francois-Gerard et al. 1979; Suzuki et al. 2001, 2003; Takahashi et al. 2001).

P1 antigenic activities have been detected in the blood and eggs of pigeons, which are considered to be a carrier of Shiga toxin-producing *Escherichia coli* (François-Gerard and Brocteur 1980; Johnson et al. 1992; Schmidt et al. 2000). The pigeon α4Gal-T used in this study has distinct and broader substrate specificity compared with the human α4Gal-T as it can transfer Gal residues to the nonreducing termini of Galβ1,4Gal, Galβ1,4Glc along with LacNAc and other monosaccharides (Suzuki and Yamamoto 2010). This explains the presence of glycoproteins with the Galα1,4Gal sequence in pigeon egg white, serum, lymphocytes and liver, whereas such mammalian glycoproteins are rare (Suzuki et al. 2003). In mammals, studies suggest that both P^k and P1 determinants are synthesized by the same α4Gal-T/Gb3 synthase that adds a galactose to lactosylceramide and paragloboside, respectively (Iwamura et al. 2003; Thuresson et al. 2011). But lactosylceramide is considered to be the favored acceptor as P^k can be synthesized even at low enzyme levels (Thuresson et al. 2011).

The choice of method (and possibly also the toxin, AB_5 or B_5) that is used to measure the binding of Stx1 and Stx2 to various defined glycan moieties clearly influences the obtained results. We observed binding of both Stx1 and Stx2 toxin (AB_5) to C-PP1 PSGL-1/mIgG_{2b} and p^k-HSA in our SPR experiments, while others failed to see any significant binding of either Stx2 or Stx2B (B_5) to P^k in ELISA experiments (Flagler et al. 2010). Recently, Gallegos et al. (2012) monitored the binding of Stx1, Stx1B, Stx2 and Stx2B with a number of different techniques. In an Isothermal titration calorimetry assay Stx1B bound to P^k with a K_D of 4 mM while no binding of Stx2B to P^k was observed (Gallegos et al. 2012). In an ELISA assay, the K_D of Stx1 binding to immobilized Gb3 was 4.2 nM while Stx2 bound very poorly. However, when mixing different proportions of glycolipids, cholesterol and phosphatidylcholine in the ELISA plate, the Stx2 binding was dramatically improved and bound with an affinity similar to that of Stx1 (Gallegos et al. 2012). Compounds like ceramide and cholesterol have previously been shown to influence binding of Stx2 to Gb3 (Lingwood et al. 2010, 2011; Mahfoud et al. 2010; Gallegos et al. 2012). It has also been shown that Stx2 preferred a P^k mimic (NAc-p^k:NAcGalα1-4Galβ1-4Glc) over native p^k (Takeda et al. 1999; Kale et al. 2008; Kitov et al. 2008; Flagler et al. 2010). So it is possible that a natural environment of the cell membrane is required for Gb3 to act as a receptor for Stx2. Although, the molecular basis of receptor recognition by Stx2 is unclear, the results of our study and other reports suggest that the binding preference of Stx2 is different from that of Stx1 (Dohi et al. 1999; Kale et al. 2008; Flagler et al. 2010). The increased risk of developing serious symptoms, including hemolytic uremic syndrome (HUS), is strongly correlated with Stx2. However, HUS has not been associated with a particular receptor on potential target cells (Bergan et al. 2012). In vitro studies have shown a lower affinity of Stx2 compared with Stx1 to Gb3, but the in vivo toxicity of Stx2 is much higher (Bergan et al. 2012). Therefore, further studies of the binding partners of Stx2 in vitro and in vivo are needed in order to design an optimal inhibitor of the Stx2 toxin.

We have previously shown that the PSGL-1/mIgG_{2b} multivalently substituted with defined carbohydrate determinants such as Galα1,3Gal, blood group ABO determinants, sialyl-Lewis x or Lewis b epitopes, and Siaα2,3Gal can be utilized as efficient human anti-αGal antibody adsorbers, anti-A/B immunoadsorbers, inhibitors of *Helicobacter pylori* binding and binders of recombinant avian H5N1 hemagglutinin, respectively (Löfling et al. 2002; Liu et al. 2003, 2005; Gustafsson et al. 2006) (S.G. manuscript in preparation). Further, the binding ability of our recombinant mucin-type fusion protein to Shiga-like toxins suggests that it might also bind to P-fimbriated uropathogenic *E. coli, Pseudomonas aeruginosa* (PA-I lectin) and *Staphylococcus aureus* (enterotoxin B) as the P1 determinant is also a functional receptor for these microbes and toxins (Bock et al. 1985; Gilboa-Garber et al. 1994; Chatterjee et al. 1995; Tikkanen et al. 1995, 1996). The productivity of the C-PP1 clone can be optimized by a second single cell cloning step and further scale up production of the mucin-type fusion protein can be done in Wave bioreactors monitoring parameters like pH, glucose (Glc) and glutamine (Gustafsson et al. 2011; Lindberg et al. 2013). The potential diagnostic and therapeutic uses of the P1-substituted mucin-type fusion protein are currently being explored.

Materials and methods

Construction of expression vector

Total RNA was extracted from pigeon liver using RNA Bee (AMS Biotechnology, Milton park, Oxfordshire, UK) and the mRNA was purified using the Poly A Tract mRNA Isolation System (cat.no.z5200, Promega Corporation, Madison, WI). Using a cDNA synthesis kit (cat.no.11117831001, Roche Applied Science, Penzberg, Germany), cDNA was prepared. The pigeon α4-galactosyltransferase gene was polymerase chain reaction-amplified using 5′-GAC AAG CTT ACC ATG TCC AGC TAC CTG CAA AAA CTG AC 3′ and 5′-TGC GGC CGC TCA CAT TAC AGG CCT TGA CTG CTC T-3′ as forward and reverse primers, respectively. The amplified cDNA of pigeon α4-galactosyltransferase was subcloned into the polylinker of CDM8 expression vector (Seed 1987; Liu et al. 1997) using *Hind*3 and *Not*1 (New England Biolabs, Beverly, MA). The vector was amplified in *E. coli* strain MC1063/P3 using 25 μg/mL ampicillin (Invitrogen) and 7.5 μg/mL tetracycline (Invitrogen) as selection drugs. The enzyme sequence was confirmed by DNA sequencing. The PSGL-1/mIgG_{2b} and C2GnT-I expression plasmids carrying puromycin and geneticin (G418 sulfate) drug resistance genes, respectively, were constructed as described before (Liu et al. 1997, 2005). The expression of the mucin-type fusion protein (PSGL-1/mIgG_{2b})

and the enzyme activity of pigeon α4-galactosyltransferase and C2GnT-I were checked by immunocytochemistry staining of transiently transfected cells using FITC-conjugated goat anti-mouse IgG (Fc) antibody (Sigma-Aldrich, St. Louis, MO) and anti-P1 antibody (Immucor gamma, Norcross), respectively.

Cell culture

The CHO-K1 cell line (cat no CCL-61; ATCC®, Manassas) was cultured in Dulbecco's modified Eagle's medium (Invitrogen) supplemented with 10% fetal bovine serum (Invitrogen), 2 mM L-glutamine (Invitrogen) and 25 µg/mL gentamicin (Invitrogen). Cells were maintained in a humidified incubator at 37°C and 5.0% CO_2.

A CHO-K1 cell line adapted to serum-free conditions were cultured in ProCHO-4 (Lonza, Basel, Switzerland) medium supplemented with 2 mM L-glutamine, 100 µg/mL dextran sulfate (Sigma-Aldrich) and 25 µg/mL gentamicin. Cells were maintained as single-cell suspension cultures in shaker flasks (Corning, Inc., NY) at 100 rpm, 37°C and 5.0% CO_2.

Stable transfection and clonal selection of glyco-engineered CHO cells

To generate stable transfectants, all the three expression vectors were linearized with *Avr*II (New England BioLabs) and the CHO-K1 cell line was seeded in a 75 cm^2 tissue culture flask on the day before transfection. The cells were transfected at 90–95% confluence with the PSGL-1/mIgG_{2b}, human C2GnT-I and the pigeon α4-galactosyltransferase expression vectors using Lipofectamine 2000™ (Invitrogen) according to the manufacturer's instructions. Twenty-four hours following transfection, the cells were split into five 100-mm tissue culture dishes and were incubated in selection medium containing 6 µg/mL puromycin, 600 µg/mL G418 and 2 µg/mL blasticidin starting 48 h after transfection. The selection medium was changed every second to third day. Drug-resistant clones were identified as colonies under the microscope after ∼2 weeks and were hand-picked using sterile pipette tips and transferred to 96-well plates in selection medium. The transfected clones were named C-PP1. Cell culture supernatants were harvested when the clones had reached 80–90% confluency, and were screened for the expression of PSGL-1/mIgG_{2b} by ELISA using a goat anti-mouse IgG Fc antibody as described in *Quantification of PSGL-1/mIgG_{2b} using ELISA*. Six high-expressing C-PP1 clones were further expanded and were analyzed again by ELISA and western blot to determine the production level of PSGL-1/mIgG_{2b} fusion protein and the presence of the P1 determinant on the recombinant fusion protein. The expression of the P1 determinant was further confirmed by immunocytochemistry staining of the cells. All the six C-PP1 clones were sequentially adapted to serum-free condition and two clones, C-PP1-A1 and C-PP1-A11, were subsequently transferred to shaker flask for large-scale cultivation. The C-P55 cell line was established by transfection of CHO-K1 with cDNA encoding the PSGL-1/mIgG_{2b} fusion protein as described previously (Lindberg et al. 2013)

Indirect immunofluorescence

The frequency of PSGL-1/mIgG_{2b} and P1 expression in transfected cells was analyzed by immunocytochemistry staining with FITC-conjugated antibodies. Cells were seeded in 6-well BD Biocoat™ plates (BD Biosciences, Franklin lakes, New Jersey) for 24–48 h of culture and then fixed in 30% ice-cold acetone in methanol (v/v) for 2 min at room temperature. Fixed cells were washed in phosphate buffered saline (PBS) and blocked in 1% BSA in PBS for 30 min. PSGL-1/mIgG_{2b} expression was detected by staining the cells with a FITC-conjugated goat anti-mouse IgG (Fc) antibody (Sigma-Aldrich) diluted 1:100. For detection of P1 expression, the cells were stained with a mouse monoclonal anti-P1 antibody (Immucor gamma) followed by a secondary FITC-conjuated goat anti-mouse IgM antibody (Sigma-Aldrich) diluted 1:200. All antibodies were diluted in 1%BSA in PBS and the incubations were performed for 1 h at room temperature in the dark. The cells were washed in PBS after each antibody incubation. As a counterstain DAPI (Invitrogen) nucleic acid stain was used at a concentration of 300 nM diluted in PBS. Cells were incubated for 1–2 min and were analyzed in a fluorescence microscope after rinsing in PBS.

Production and purification of secreted PSGL-1/mIgG_{2b} fusion protein

Clone C-PP1-A1 and C-PP1-A11 was cultured in serum-free ProCHO-4 medium (Lonza) in 3 L shaker flasks (Corning) at 100 rpm and 37°C with 5% CO_2. The culture was harvested when the final cell density had reached 3–4 × 10^6 cells/mL and the viability had dropped to 70%. The cell culture supernatant containing PSGL-1/mIg$G2_b$ with P1 epitope were cleared by centrifugation and further clarified by filtration.

All chromatographic procedures were carried out on an ÄKTAExplorer 100 controlled by the Unicorn software (v. 5.11) (GE Healthcare, Uppsala, Sweden). The clarified supernatants were sterile filtered with a 0.22 µm polyether sulfone filter (Nalgene, Thermo Fisher Scientific, San Jose, CA) before loading onto a MabSelect SuRe column (GE Healthcare) preequilibrated with PBS. The column was washed with 10 column volumes (CV) of PBS, and elution of recombinant fusion protein was achieved using 5 CV of 0.1 M sodium citrate, pH 3.0. After elution, selected fractions were pooled, neutralized with 300 µL per mL of 1 M Tris–HCl, pH 9.0, and then dialyzed extensively (12–14 kD cut-off) against MilliQ water at 4°C. After dialysis, the samples were frozen, lyophilized and stored at −80°C before further purification.

Lyophilized samples were dissolved to ∼5 mg/mL in gel filtration buffer (0.1 M sodium phosphate, pH 7.2, 0.5 M sodium chloride). Gel filtration of the PSGL-1/mIgG_{2b} was carried out on a preequilibrated HiPrep 26/60 Sephacryl S-300 HR column (GE Healthcare). Typically, 5 mL sample was applied to the gel filtration column and eluted with a flow rate of 1 mL/min. Eluted fractions were kept at 4°C until pooling was done on the basis of western blot analysis. Pooled fractions were then dialyzed Phosphate buffered saline as above, frozen, lyophilized and stored at −80°C. Production and purification of PSGL-1/mIgG_{2b} derived from the C-P55 cell line has been described in detail previously (Lindberg et al. 2013).

Quantification of PSGL-1/mIgG$_{2b}$ using ELISA

The concentrations of recombinant fusion protein in supernatants and in purified fractions were determined by a two-antibody sandwich ELISA method as described previously (Gustafsson et al. 2011).

PNGase F-treatment

Purified PSGL-1/mIgG$_{2b}$ was subjected to PNGase F digestion (*N*-Glycosidase F Deglycosylation kit, Roche Applied Science) according to the manufacturer's instructions. After 1 h of digestion at 37°C, the samples were analyzed on SDS–PAGE and western blotting as described below.

SDS–PAGE and western blotting

PSGL-1/mIgG$_{2b}$ purified from cell culture supernatants on goat anti-mouse IgG agarose beads (Sigma-Aldrich) by the manufacturer's instructions and by chromatographic procedures in large scale were analyzed by SDS–PAGE under nonreducing conditions using 3–8% Tris-acetate gradient gels and Tris-acetate SDS running buffer (Invitrogen). Precision protein standard (Hi-Mark, Invitrogen) was applied as reference for protein molecular weight determination. Separated proteins were electrophoretically blotted using iBlot (Invitrogen) in combination with nitrocellulose membranes (Invitrogen). The membranes were blocked with 3% BSA in PBS with 0.2% Tween 20, which was also used for dilution of antibodies. Western blot membranes were probed with a peroxidase-conjugated anti-mouse IgG(Fc) (Sigma-Aldrich), mouse anti-PSGL-1 antibody (clone KPL-1, BD PharMingen, San Diego, CA) and anti-P1 antibody (Immucor gamma). Secondary antibodies for detecting PSGL-1 and P1 epitope were peroxidase-conjugated goat anti-mouse IgG F(ab)′$_2$ (Sigma-Aldrich) and goat anti-mouse IgM-HRP, respectively. Bound antibodies were visualized by chemiluminescence using the ECL kit according to the manufacturer's instructions (GE Healthcare).

To detect the glycosylated protein, the SDS–PAGE Protein gels were stained using the Pro Q Emerald 300 Glycoprotein detection kit in combination with Ruby (Molecular Probes, Leiden, Netherlands). The Candycane precision standard (Invitrogen) was applied as a reference for protein molecular weight determination. These gels were visualized in a Flour-S Max MultiImager carrying a CCD camera (Bio-Rad, Hercules, CA).

Chemical release of O-linked glycans from purified PSGL-1/mIgG$_{2b}$ carrying P1 epitope

O-glycans were released from the purified PSGL-1/mIgG$_{2b}$ protein by β-elimination in a solution of 0.5 M $NaBH_4$ in 50 mM KOH, as described previously (Kenny et al. 2012). Briefly, the released *O*-glyans were desalted on a home-made cation exchange column with AG50WX8 beads (Bio-Rad) packed on a C18 zip-tip (Millipore, Billerica, MA). The borate complexes were removed with successive washing/evaporation steps in 1% acetic acid in methanol. The *O*-glycans were dissolved in water and injected into the LC-MS instrument.

Mass spectrometry

The released O-glycans were analyzed with LC-MS and LC-MS2 using a graphitized carbon column coupled to an LTQ LC/MS^n ion trap instrument (Thermo Scientific, Waltham, MA), as described previously by Karlsson et al. (2004). The column was packed with 5 µm Hypercarb particles (Thermo, Hypersil-Keystone, Runcorn, UK). A gradient from 0 to 40% acetonitrile in 8 mM NH_4HCO_3 buffer eluted the glycans which were detected in negative mode by full scans (*m/z* 383–2000) followed by MS^2 scans of the most intense ions. The needle voltage was −3.2 kV.

Interpretation of mass spectra

The original spectra were imported into GlycoWorkBench (downloadable free java tool, http://download.glycoworkbench.org/ (Ceroni et al. 2007, 2008). The fragment tool of the program was used to calculate the B, C, Z, Y and cross-ring fragments of drawn structures. The fragments were matched with the peak lists using the annotate tool. The LC-MS^2 spectra for all structures listed in this paper were submitted to UniCarb-DB (www.unicarb-db.com) to allow access to the full dataset (Hayes et al. 2011).

Neoglycoconjugates and Shiga toxins

p^k-HSA (Galα1,4Galβ1,4Glc3-atom spacer-NH-HSA) and P1-BSA (Galα1,4Galβ1,4GlcNAcβ1,3Galβ1,4Glc3-atom spacer-NH-HSA) were acquired from Dextra Laboratories (Reading, UK). The p^k-HSA neoglycoconjugate has a mass of 73,534 Dalton and an average substitution grade of 12.7 mol carbohydrate/mol protein (minimum 8 and maximum 19) as determined by laser desorption time of flight MS. Purity was reported to be >95%. The P1-BSA neoglycoconjugate acquired from Calbiochem has an average substitution grade of 10–12 mol carbohydrate/mol protein. Stx1 and Stx2 toxins, both of purity 50 and 95%, were purchased from Toxin Technology (Sarosta, FL). The approximate purity of the toxin was determined by SDS–PAGE and the toxicity as assessed in a Vero Cell Assay was greater than 10^7 Units per milligram according to the manufacturer.

Shiga toxin immunoblotting

SDS–PAGE and western blotting was run under the same conditions as above. Stx1 (Toxin Technology) binding was detected by incubating the membrane with both highly purified (95%) and partially purified Stx1 (50%) followed by anti-Stx1 antibody (STX1-3C10, Toxin Technology) and goat anti-mouse IgG(Fab)-HRP (Sigma). Visualization was performed as above (see section SDS–PAGE and western blotting). P1-BSAand p^k-HSA were used as positive controls and fusion protein (C-P55) produced from CHO-K1 cells stably transfected with PSGL-1/mIgG$_{2b}$ alone were used as negative control.

Real-time SPR analysis

The analyses were performed using a Biacore 2000 instrument with a research-grade CM5 sensor chip (Biacore, GE Healthcare). The ligand Stx1 (Stx1, Toxin Technology) (theoretical AB_5 mass 70.7 kDa, >95% pure) was immobilized using amine coupling chemistry according to the manufacturer's instructions. Briefly, the surfaces were activated for 7 min with a 1:1 mixture of 0.1 M N-hydroxysuccinimide and 0.1 M 1-ethyl-3-(3-dimethylaminopropyl)carbodiimide hydrochloride (EDC) at a flow rate of 5 µL/min. The Stx1 ligand was injected at a concentration of 6.5 µg/mL in 10 mM sodium acetate buffer, pH 5.5

(GE Healthcare), for 25 min at a 5 µL/mL flow rate resulting in a density of ~2800 RU. Stx2 (theoretical AB_5 mass 72.2 kDa, >95% pure) was immobilized with injection at 13 µg/mL in 10 mM sodium acetate buffer, pH 5.5, for 25 min at a 5 µL/mL flow rate resulting in a density of ~2000 RU. Channel one on the CM5 sensor chip was only activated/deactivated and was used as reference sensorgram for subtraction of buffer effects. All the used surfaces were blocked with a 7 min injection of 1 M ethanolamine, pH 8.0. The analytes (C-PP1-A1 (300 kDa), P-PM (250 kDa) and p^k-HSA (73.5 kDa) were dissolved in running buffer HBS-EP (10 mM (4-(2-hydroxyethyl)-1-piperazineethanesulfonic acid) [HEPES], 150 mM NaCl, 0.005% P20, pH 7.4), GE Healthcare) supplemented with 0.05% P20 and injected over the flow cells in a concentration series of 0.14, 0.4, 1.2, 3.7, 11, 33, 100, 300, 900 and 2700 nM at a flow rate of 20 µL/min at a temperature of 25°C. The association complex was built up during 600 s and the dissociated for 600 s. The Stx1 surface was regenerated with 30 s injection of 5 mM Glycin-HCl, pH 3.2, 0.5 M $MgCl_2$ (GE Healthcare) followed by 5 min stabilization time for the PP1 fusion protein analyte. For the p^k-HSA analyte, a 5 mM Glycin-HCl, pH 3.2, 1.0 M $MgCl_2$ regeneration solution was used. Samples were injected in order of increasing concentration with at least one duplicate and several buffer blanks. Data were collected at 1 Hz and fitted using a 1:1 interaction model available in the Scrubber 2 software.

Estimations of affinity

The calculated affinity values rely on the concentrations of PSGL-1/mIgG_{2b} determined with ELISA and the estimated molecular weight of 300 kDa from migration on SDS–PAGE. The steady-state calculations were determined from 550 to 600 s sections of the binding curves using a simple 1:1 fit available in the Scrubber 2 software.

Funding

This work was supported by the Swedish Research Council (K2011-65X-3031-01-6 to J.H. and 621-2010-5322 to N.G. K.), the County Council of Västra Götaland (ALF) to J.H, Swedish Governmental Agency for Innovation Systems (2010-00528) and Karolinska Institute Faculty funds (KID-funding) to S.G. The mass spectrometer was obtained by a grant from the Swedish Research Council (342-2004-4434).

Acknowledgements

The authors thank Dr. Chunsheng Jin (Department of Medical Biochemistry, Sahlgrenska Academy, Sweden) for support in liquid chromatography—mass spectroscopy analysis, Dr. Linda Lindberg (Cepheid, Sweden) for helpful discussions and Recopharma AB (Sweden) for providing C-P55-derived PSGL-1/mIgG_{2b} and Laboratory support for cell culture and protein purification.

Conflicts of interest

J.H. is a part time CEO/CSO, board member and shareholder of Recopharma AB, Sweden. A.N. is an employee of Recopharma AB. All other authors (R.M.C., S.G., J.L., N.K.) declare no conflict of interest.

Abbreviations

C2GnT-I, core 2 β1,6-*N*-acetylglucosaminyltransferase; CHO-K1, Chinese hamster ovary cells K-1; CV, column volumes; DAP1, 4′,6-diamidino-2-phenylindole; EDC, 1-ethyl-3-(3-dimethylaminopropyl)carbodiimide hydrochloride; ELISA, enzyme-linked immunosorbent assay; FITC, fluorescein isothiocyanate; Gal, galactose; GalNAc, *N*-acetylgalactosamine; Gb3, Globotriaosylceramide; GB4, Globotetraosylceramide; Glc, glucose; GlcNAc, *N*-acetylglucosamine; HEPES, 4-(2-hydroxyethyl)-1-piperazineethanesulfonic acid; HexNAc, *N*-acetylhexosamine; HSA, human serum albumin; HUS, hemolytic uremic syndrome; LC, liquid chromatography; MS, mass spectrometry; P1-BSA, P1 determinant conjugated to bovine serum albumin; PBS, phosphate buffered saline; PNGase F, *N*-glycosidase F; PSGL-1/mIgG_{2b}, P-selectin glycoprotein ligand-1/mouse IgG_{2b}; Sia, sialic acid; SPR, surface plasmon resonance; Stx1, Shiga-like toxin 1; Stx2, Shiga-like toxin 2; α4Gal-T, α1,4-galactosyltransferase.

References

Bergan J, Dyve Lingelem AB, Simm R, Skotland T, Sandvig K. 2012. Shiga toxins. *Toxicon*. 60:1085–1107.

Bock K, Breimer ME, Brignole A, Hansson GC, Karlsson KA, Larson G, Leffler H, Samuelsson BE, Stromberg N, Eden CS. 1985. Specificity of binding of a strain of uropathogenic *Escherichia coli* to Gal alpha 1—4Gal-containing glycosphingolipids. *J Biol Chem*. 260:8545–8551.

Ceroni A, Dell A, Haslam SM. 2007. The GlycanBuilder: A fast, intuitive and flexible software tool for building and displaying glycan structures. *Source Code Biol Med*. 2:3.

Ceroni A, Maass K, Geyer H, Geyer R, Dell A, Haslam SM. 2008. GlycoWorkbench: A tool for the computer-assisted annotation of mass spectra of glycans. *J Proteome Res*. 7:1650–1659.

Chatterjee S, Khullar M, Shi WY. 1995. Digalactosylceramide is the receptor for staphylococcal enterotoxin-B in human kidney proximal tubular cells. *Glycobiology*. 5:327–333.

DeGrandis S, Law H, Brunton J, Gyles C, Lingwood CA. 1989. Globotetraosylceramide is recognized by the pig edema disease toxin. *J Biol Chem*. 264:12520–12525.

Dohi H, Nishida Y, Mizuno M, Shinkai M, Kobayashi T, Takeda T, Uzawa H, Kobayashi K. 1999. Synthesis of an artificial glycoconjugate polymer carrying Pk-antigenic trisaccharide and its potent neutralization activity against Shiga-like toxin. *Bioorg Med Chem*. 7:2053–2062.

Dundas S, Todd WTA, Stewart AI, Murdoch PS, Chaudhuri AKR, Hutchinson SJ. 2001. The central Scotland *Escherichia coli* O157:H7 outbreak: Risk factors for the hemolytic uremic syndrome and death among hospitalized patients. *Clin Infect Dis*. 33:923–931.

Endo Y, Tsurugi K, Yutsudo T, Takeda Y, Ogasawara T, Igarashi K. 1988. Site of action of a Vero toxin (VT2) from *Escherichia coli* O157:H7 and of Shiga toxin on eukaryotic ribosomes. *Eur J Biochem*. 171:45–50.

Flagler MJ, Mahajan SS, Kulkarni AA, Iyer SS, Weiss AA. 2010. Comparison of binding platforms yields insights into receptor binding differences between shiga toxins 1 and 2. *Biochemistry*. 49:1649–1657.

François-Gerard C, Brocteur J. 1980. Application à la sérologie transfusionnelle du caractère antigénique P1 du blanc d'œuf de pigeon. *Rev Fr Transfus Immunohematol*. 23:95–102.

Francois-Gerard C, Gerday C, Beeley JG. 1979. Turtle-dove ovomucoid, a glycoprotein proteinase inhibitor with P1-blood-group antigen activity. *Biochem J*. 177:679–685.

Fraser ME, Chernaia MM, Kozlov YV, James MN. 1994. Crystal structure of the holotoxin from Shigella dysenteriae at 2.5 A resolution. *Nat Struct Biol*. 1:59–64.

Gallegos KM, Conrady DG, Karve SS, Gunasekera TS, Herr AB, Weiss AA. 2012. Shiga toxin binding to glycolipids and glycans. *PLoS One*. 7:e30368.

Gilboa-Garber N, Sudakevitz D, Sheffi M, Sela R, Levene C. 1994. PA-I and PA-II lectin interactions with the ABO(H) and P blood group glycosphingolipid antigens may contribute to the broad spectrum adherence of *Pseudomonas aeruginosa* to human tissues in secondary infections. *Glycoconj J*. 11:414–417.

Gustafsson A, Hultberg A, Sjöström R, Kacskovics I, Breimer ME, Borén T, Hammarström L, Holgersson J. 2006. Carbohydrate-dependent inhibition of *Helicobacter pylori* colonization using porcine milk. *Glycobiology*. 16:1–10.

Gustafsson A, Sjoblom M, Strindelius L, Johansson T, Fleckenstein T, Chatzissavidou N, Lindberg L, Angstrom J, Rova U, Holgersson J. 2011. Pichia pastoris-produced mucin-type fusion proteins with multivalent O-glycan substitution as targeting molecules for mannose-specific receptors of the immune system. *Glycobiology*. 21:1071–1086.

Hayes CA, Karlsson NG, Struwe WB, Lisacek F, Rudd PM, Packer NH, Campbell MP. 2011. UniCarb-DB: A database resource for glycomic discovery. *Bioinformatics*. 27:1343–1344.

Iwamura K, Furukawa K, Uchikawa M, Sojka BN, Kojima Y, Wiels J, Shiku H, Urano T, Furukawa K. 2003. The blood group P1 synthase gene is identical to the Gb3/CD77 synthase gene. A clue to the solution of the P1/P2/p puzzle. *J Biol Chem*. 278:44429–44438.

Johannes L, Romer W. 2010. Shiga toxins–from cell biology to biomedical applications. *Nat Rev Microbiol*. 8:105–116.

Johnson JR, Berggren T. 1994. Pigeon and dove eggwhite protect mice against renal infection due to P fimbriated *Escherichia coli*. *Am J Med Sci*. 307:335–339.

Johnson JR, Ross AE. 1993. P1-antigen-containing avian egg whites as inhibitors of P adhesins among wild-type *Escherichia coli* strains from patients with urosepsis. *Infect Immun*. 61:4902–4905.

Johnson JR, Swanson JL, Neill MA. 1992. Avian P1 antigens inhibit agglutination mediated by P fimbriae of uropathogenic *Escherichia coli*. *Infect Immun*. 60:578–583.

Kale RR, McGannon CM, Fuller-Schaefer C, Hatch DM, Flagler MJ, Gamage SD, Weiss AA, Iyer SS. 2008. Differentiation between structurally homologous Shiga 1 and Shiga 2 toxins by using synthetic glycoconjugates. *Angew Chem Int Ed*. 47:1265–1268.

Karlsson NG, Schulz BL, Packer NH. 2004. Structural determination of neutral O-linked oligosaccharide alditols by negative ion LC-electrospray-MSn. *J Am Soc Mass Spectrom*. 15:659–672.

Karmali MA, Steele BT, Petric M, Lim C. 1983. Sporadic cases of haemolytic-uraemic syndrome associated with faecal cytotoxin and cytotoxin-producing *Escherichia coli* in stools. *Lancet*. 1:619–620.

Kenny DT, Skoog EC, Lindén SK, Struwe WB, Rudd PM, Karlsson NG. 2012. Presence of terminal N-acetylgalactosamineβ1-4N-acetylglucosamine residues on O-linked oligosaccharides from gastric MUC5AC: Involvement in *Helicobacter pylori* colonization? *Glycobiology*. 22:1077–1085.

Kitov PI, Mulvey GL, Griener TP, Lipinski T, Solomon D, Paszkiewicz E, Jacobson JM, Sadowska JM, Suzuki M, Yamamura K, et al. 2008. In vivo supramolecular templating enhances the activity of multivalent ligands: A potential therapeutic against the *Escherichia coli* O157 AB5 toxins. *P Natl Acad Sci USA*. 105:16837–16842.

Kitov PI, Sadowska JM, Mulvey G, Armstrong GD, Ling H, Pannu NS, Read RJ, Bundle DR. 2000. Shiga-like toxins are neutralized by tailored multivalent carbohydrate ligands. *Nature*. 403:669–672.

Li X, Wu P, Cheng S, Lv X. 2012. Synthesis and assessment of globotriose-chitosan conjugate, a novel inhibitor of shiga toxins produced by *Escherichia coli*. *J Med Chem*. 55:2702–2710.

Lindberg AA, Brown JE, Stromberg N, Westling-Ryd M, Schultz JE, Karlsson KA. 1987. Identification of the carbohydrate receptor for Shiga toxin produced by Shigella dysenteriae type 1. *J Biol Chem*. 262:1779–1785.

Lindberg L, Liu J, Gaunitz S, Nilsson A, Johansson T, Karlsson NG, Holgersson J. 2013. Mucin-type fusion proteins with blood group A or B determinants on defined O-glycan core chains produced in glycoengineered Chinese hamster ovary cells and their use as immunoaffinity matrices. *Glycobiology*. 23:720–735.

Ling H, Boodhoo A, Hazes B, Cummings MD, Armstrong GD, Brunton JL, Read RJ. 1998. Structure of the shiga-like toxin I B-pentamer complexed with an analogue of its receptor Gb3. *Biochemistry*. 37:1777–1788.

Lingwood CA. 1993. Verotoxins and their glycolipid receptors. *Adv Lipid Res*. 25:189–211.

Lingwood CA, Binnington B, Manis A, Branch DR. 2010. Globotriaosyl ceramide receptor function—Where membrane structure and pathology intersect. *FEBS Lett*. 584:1879–1886.

Lingwood D, Binnington B, Rog T, Vattulainen I, Grzybek M, Coskun U, Lingwood CA, Simons K. 2011. Cholesterol modulates glycolipid conformation and receptor activity. *Nat Chem Biol*. 7:260–262.

Liu J, Gustafsson A, Breimer ME, Kussak A, Holgersson J. 2005. Anti-pig antibody adsorption efficacy of α-Gal carrying recombinant P-selectin glycoprotein ligand-1/immunoglobulin chimeras increases with core 2 β1, 6-N-acetylglucosaminyltransferase expression. *Glycobiology*. 15:571–583.

Liu J, Qian Y, Holgersson J. 1997. Removal of xenoreactive human anti-pig antibodies by absorption on recombinant mucin-containing glycoproteins carrying the Gal alpha1,3Gal epitope. *Transplantation*. 63:1673–1682.

Liu J, Weintraub A, Holgersson J. 2003. Multivalent Galalpha1,3Gal-substitution makes recombinant mucin-immunoglobulins efficient absorbers of anti-pig antibodies. *Xenotransplantation*. 10:149–163.

Löfling JC, Hauzenberger E, Holgersson J. 2002. Absorption of anti-blood group A antibodies on P-selectin glycoprotein ligand-1/immunoglobulin chimeras carrying blood group A determinants: Core saccharide chain specificity of the Se and H gene encoded α1,2 fucosyltransferases in different host cells. *Glycobiology*. 12:173–182.

MacConnachie AA, Todd WT. 2004. Potential therapeutic agents for the prevention and treatment of haemolytic uraemic syndrome in shiga toxin producing *Escherichia coli* infection. *Curr Opin Infect Dis*. 17:479–482.

Mahfoud R, Manis A, Binnington B, Ackerley C, Lingwood CA. 2010. A major fraction of glycosphingolipids in model and cellular cholesterol-containing membranes is undetectable by their binding proteins. *J Biol Chem*. 285:36049–36059.

Miyake M, Utsuno E, Noda M. 2000. Binding of avian ovomucoid to Shiga-like toxin type 1 and its utilization for receptor analog affinity chromatography. *Anal Biochem*. 281:202–208.

Schmidt H, Scheef J, Morabito S, Caprioli A, Wieler LH, Karch H. 2000. A new Shiga toxin 2 variant (Stx2f) from *Escherichia coli* isolated from pigeons. *Appl Environ Microbiol*. 66:1205–1208.

Schulz BL, Packer NH, Karlsson NG. 2002. Small-scale analysis of O-linked oligosaccharides from glycoproteins and mucins separated by gel electrophoresis. *Anal Chem*. 74:6088–6097.

Seed B. 1987. An LFA-3 cDNA encodes a phospholipid-linked membrane protein homologous to its receptor CD2. *Nature*. 329:840–842.

Shimizu H, Field RA, Homans SW, Donohue-Rolfe A. 1998. Solution structure of the complex between the B-subunit homopentamer of verotoxin VT-1 from *Escherichia coli* and the trisaccharide moiety of globotriaosylceramide. *Biochemistry*. 37:11078–11082.

Stein PE, Boodhoo A, Tyrrell GJ, Brunton JL, Read RJ. 1992. Crystal structure of the cell-binding B oligomer of verotoxin-1 from E. coli. *Nature*. 355:748–750.

Suzuki N, Khoo K, Chen C, Chen H, Lee YC. 2003. N-glycan structures of pigeon IgG. *J Biol Chem*. 278:46293–46306.

Suzuki N, Khoo K, Chen H, Johnson JR, Lee YC. 2001. Isolation and characterization of major glycoproteins of pigeon egg white. *J Biol Chem*. 276:23221–23229.

Suzuki N, Yamamoto K. 2010. Molecular cloning of pigeon UDP-galactose:β-d-galactoside α1,4-galactosyltransferase and UDP-galactose:β-d-galactoside β1,4-galactosyltransferase, two novel enzymes catalyzing the formation of Galα1–4Galβ1–4Galβ1–4GlcNAc sequence. *J Biol Chem*. 285:5178–5187.

Takahashi N, Khoo K, Suzuki N, Johnson JR, Lee YC. 2001. N-glycan structures from the major glycoproteins of pigeon egg white. *J Biol Chem*. 276:23230–23239.

Takeda T, Yoshino K, Adachi E, Sato Y, Yamagata K. 1999. In vitro assessment of a chemically synthesized Shiga toxin receptor analog attached to chromosorb P (Synsorb Pk) as a specific absorbing agent of Shiga toxin 1 and 2. *Microbiol Immunol*. 43:331–337.

Tesh VL, O'Brien AD. 1991. The pathogenic mechanisms of Shiga toxin and the Shiga-like toxins. *Mol Microbiol*. 5:1817–1822.

Thuresson B, Westman JS, Olsson ML. 2011. Identification of a novel A4GALT exon reveals the genetic basis of the P1/P2 histo-blood groups. *Blood*. 117:678–687.

Tikkanen K, Haataja S, Finne J. 1996. The galactosyl-(alpha 1–4)-galactose-binding adhesin of *Streptococcus suis*: Occurrence in strains of different hemagglutination activities and induction of opsonic antibodies. *Infect Immun*. 64:3659–3665.

Tikkanen K, Haataja S, Francois-Gerard C, Finne J. 1995. Purification of a galactosyl-alpha 1–4-galactose-binding adhesin from the gram-positive meningitis-associated bacterium Streptococcus suis. *J Biol Chem*. 270: 28874–28878.

Tomoda H, Arai M, Koyama N, Matsui H, Ō mura S, Obata R, Lee YC. 2002. Purification of Shiga-like toxin 1 by pigeon egg white glycoproteins immobilized on Sepharose gels. *Anal Biochem*. 311:50–56.

Varki A, Cummings RD, Esko JD, Freeze HH, Stanley P, Marth JD, Bertozzi CR, Hart GW, Etzler ME. 2009. Symbol nomenclature for glycan representation. *Proteomics*. 9:5398–5399.